The Fundamental Plane of evolving red nuggets

Oldham, Lindsay; Auger, Matthew; Fassnacht, Christopher D.; Treu, Tommaso; Koopmans, L. V. E.; Lagattuta, David; McKean, John; Vegetti, Simona

[Link to publication in University of Groningen/UMCG research database](#)

The Fundamental Plane of evolving red nuggets

Lindsay Oldham,[1][*] Matthew Auger,[1] Christopher D. Fassnacht,[2] Tommaso Treu,[3] L. V. E. Koopmans,[4] David Lagattuta,[5] John McKean[4,6] and Simona Vegetti[7]

[1]*Institute of Astronomy, University of Cambridge, Madingley Road, Cambridge CB3 0HA, UK*
[2]*Department of Physics, University of California, Davis, 1 Shields Ave., Davis, CA 95616, USA*
[3]*Department of Physics and Astronomy, UCLA, 430 Portola Plaza, Los Angeles, CA 90095-1547, USA*
[4]*Kapteyn Astronomical Institute, University of Groningen, PO Box 800, NL-9700 AV Groningen, the Netherlands*
[5]*CNRS, Centre de Recherche Astrophysique de Lyon UMR5574, Université de Lyon, F-69230 Saint-Genis-Laval, France*
[6]*ASTRON, Netherlands Institute for Radio Astronomy, Postbus 2, NL-7990 AA Dwingeloo, the Netherlands*
[7]*Max Planck Institute for Astrophysics, Karl-Schwarzschild-Strasse 1, D-85740 Garching, Germany*

ABSTRACT

We present an exploration of the mass structure of a sample of 12 strongly lensed massive, compact early-type galaxies at redshifts $z \sim 0.6$ to provide further possible evidence for their inside-out growth. We obtain new Echelette Spectrograph and Imager/Keck spectroscopy and infer the kinematics of both lens and source galaxies, and combine these with existing photometry to construct (a) the Fundamental Plane (FP) of the source galaxies and (b) physical models for their dark and luminous mass structure. We find their FP to be tilted towards the virial plane relative to the local FP, and attribute this to their unusual compactness, which causes their kinematics to be totally dominated by the stellar mass as opposed to their dark matter; that their FP is nevertheless still inconsistent with the virial plane implies that both the stellar and dark structure of early-type galaxies is non-homologous. We also find the intrinsic scatter of their FP to be comparable to the local value, indicating that variations in the stellar mass structure outweigh variations in the dark halo in the central regions of early-type galaxies. Finally, we show that inference on the dark halo structure – and, in turn, the underlying physics – is sensitive to assumptions about the stellar initial mass function (IMF), but that physically motivated assumptions about the IMF imply haloes with sub-Navarro–Frenk–White inner density slopes, and may present further evidence for the inside-out growth of compact early-type galaxies via minor mergers and accretion.

Key words: gravitational lensing: strong – galaxies: elliptical and lenticular, cD – galaxies: evolution – galaxies: kinematics and dynamics – galaxies: structure.

1 INTRODUCTION

The discovery that massive, passive galaxies at redshifts $z \sim 2$ are much more compact than their present-day counterparts (Daddi et al. 2005; Trujillo et al. 2006; van Dokkum et al. 2008) has led to a picture in which early-type galaxies (ETGs) evolve dramatically in size over the course of their lives. Moreover, the detection of extended outer envelopes surrounding lower redshift compact ETGs (van Dokkum & Conroy 2010; Oldham et al. 2017a) implies an important role for dissipationless merging and accretion in evolving these systems towards the present-day size–mass relation. However, though a consensus is now building over the evolution of their luminous structure, their dark halo structure remains elusive.

Even in normal (non-compact) ETGs, how the dark halo is affected by baryonic processes such as mergers and accretion is not well understood; simulations suggest that dynamical heating from infalling satellites should displace dark matter from the centre of the halo to larger radii (El-Zant et al. 2004; Laporte et al. 2012), but this must compete with other processes such as adiabatic contraction during the infall of stellar material and feedback from supernovae and active galactic nuclei (Read & Gilmore 2005; Martizzi, Teyssier & Moore 2013). Observationally, the picture is also unclear, with the halo structure of ETGs exhibiting a diversity which may depend on environment (Newman, Ellis & Treu 2015; Oldham & Auger 2016). Probing the mass structure of low redshift, partly evolving massive compact 'red nugget' galaxies, where the evolution of the baryonic material is dominated by merging, allows us to isolate this aspect of inside-out growth from other baryonic processes and investigate its impact on the haloes of individual galaxies much more closely.

* E-mail: ljo31@ast.cam.ac.uk

The mass structure of ETGs *as a population*, on the other hand, has historically been accessed through the Fundamental Plane (FP) which tightly relates their characteristic size, velocity dispersion and surface brightness (Djorgovski & Davis 1987; Dressler et al. 1987). The existence of such a plane follows directly from the assumption that galaxies are virialized – and, to some extent, homologous – systems (see e.g. Ciotti, Lanzoni & Renzini 1996), with the small intrinsic scatter indicating a strong degree of regularity in their formation and evolution. However, the fact that the FP is tilted relative to the virial prediction implies some degree of non-homology, with mass-dependent variations in either the luminous matter – for instance, the stellar initial mass function (IMF), stellar mass structure and stellar dynamics – or the dark matter – including the dark halo structure, concentration and the dark matter fraction – or both; however, it is difficult to disentangle effects of variations in the dark and light structure (see e.g. Trujillo, Burkert & Bell 2004; Cappellari et al. 2006; La Barbera et al. 2008) so as to extract information on galaxy structure (though the construction of the *mass plane* has helped to discount dynamical non-homology as the main cause of the FP tilt; see Bolton et al. 2008). Constructing the FP for compact galaxies, whose luminosity-weighted velocity dispersions probe the very central regions where the dark matter fraction is expected to be low, provides a way to separate the contributions to the FP tilt from the stars and the halo and so better understand the mass properties of the ETG population.

In this paper, we present a new high signal-to-noise Echelette Spectrograph and Imager (ESI)/Keck spectroscopy for the 13 early-type/early-type lenses (EELs) of Oldham et al. (2017a), and combine these data with photometry to probe the mass structure of both the individual galaxies and the population as a whole. The background galaxies of the EELs are massive and compact ETGs, which the combination of lensing magnification and high-resolution imaging data can resolve on ∼100 pc scales, making them the ideal sample with which to probe ETG structural evolution. In Section 2, we introduce the data, the data reduction and the kinematic modelling. Section 3 presents the FP; in Section 4 we construct physical models of the EELs sources in order to set constraints on their dark matter content, and in Section 5 we discuss our findings and conclude. Throughout the paper, we use circularized radii and assume a flat Λ cold dark matter cosmology with $\Omega_m = 0.3$ and $h = 0.7$.

2 DATA AND KINEMATIC MODELLING

We observed the 13 EELs using the ESI (Sheinis et al. 2002) on Keck on the nights of 2013 May 14, 2015 January 23 and 2016 July 8, obtaining 1 h exposures for each system (except J1218+5648, J1605+3811 and J2228−0018, which were observed for 30, 10 and 10 min, respectively), using a slit width of 0.75 arcsec. The data were reduced with a custom-made, PYTHON-based pipeline and the wavelength scale calibrated using arc lamp exposures taken on the night. For each system, we extracted spectra over two separate apertures – one centred on the lens with width 0.5 arcsec and a second centred on the brightest part of the Einstein ring with width 0.3 arcsec – to obtain spectra which maximized the relative signal from the lens and the source, respectively. For one system (J1606+2235), the slit did not cover the surface brightness peaks in the source galaxy which meant that we were not able to extract a spectrum of the central regions of the source in this case; we therefore exclude it from our sample. The source galaxy spectra for the 12 remaining systems are presented in Fig. 1.

To determine the stellar velocity dispersions, we model each spectrum as the sum of a lens, source and additive continuum com-

ponent. For the lens and source, we use stellar templates for A, F, G and K stars from the Indo-US Stellar Library of Coudé Feed Stellar Spectra (Valdes et al. 2004), which we redshift and convolve with a dispersion $\sigma_{model}^2 = \sigma_{true}^2 + \sigma_{inst}^2 - \sigma_{tmp}^2$, where σ_{true} is the physical velocity dispersion of the system, $\sigma_{inst} = 20.30$ km s^{-1} is the instrument resolution and σ_{tmp} is the intrinsic resolution of the templates (which is 1.2 Å for the Indo-US templates). The continuum is an order-6 polynomial that accounts for the difference in shape between the templates and the true spectrum, and regions where atmospheric absorption dominates the spectrum are masked. We therefore have four free non-linear parameters – the redshift and velocity dispersion for each of the lens and the source – and 24 linear parameters – the weights of each of the nine stellar templates for the source and the lens (4 K stars, 3 G stars and one A and F star each), and the coefficients of the order-6 polynomial – which we explore using the Markov chain Monte Carlo (MCMC) package EM-CEE (Foreman-Mackey et al. 2013). Our kinematic models are also shown in Fig. 1 and the kinematics for the sources, together with their photometric properties, are summarized in Table 1. We defer the presentation of the lens galaxy kinematics to a future work.

We test the robustness of our kinematic inference by repeating the modelling process using the lower resolution galaxy templates of Bruzual & Charlot (2003) and find that the typical uncertainty in the velocity dispersion of the source is of the order of 5 per cent; as this is significantly larger than our statistical uncertainties, we impose this as the uncertainty on all our velocity dispersion measurements. We also check the robustness of our method by modelling the kinematics of (a) the ESI spectra, extracted over apertures of width 1.5 arcsec, centred on the lens (to emulate the SDSS apertures, which are circular with radius 1.5 arcsec) and (b) the actual SDSS spectra, and compare our inference on the lens kinematics in each case; the uncertainty indicated by these tests is typically smaller than the uncertainty due to the choice of templates.

We combine these kinematics with the photometry presented in Oldham et al. (2017a) in order to construct both the FP and physical mass models. In that paper, parametric light and lensing mass distributions were used to model the *Hubble Space Telescope* (*HST*)/ACS, V/I and Keck/NIRC2 K′ imaging of the 13 EEL systems. We refer the reader to that paper for full details on the modelling and results, but note that here we use the photometric models that allow the source galaxies to have two Sérsic components (labelled '2C models' in that paper) as, for some systems, the one-component models do not provide an adequate description of the light profile (leading to large differences between one-component and two-component size measurements for a small number of objects). We summarize the effective radii R_e and effective surface brightnesses $\log I_e$ (defined as the average surface brightness within the effective radius, evaluated in the rest-frame Johnson V band using the photometric models of Oldham et al. 2017a) in Table 1.

3 FUNDAMENTAL PLANE

3.1 The observed Fundamental Plane

We model the FP for the 12 EELs sources as

$$\log R_e = \alpha \log \sigma + \beta \log I_e + \gamma \qquad (1)$$

for effective radius R_e in kpc, velocity dispersion σ in units of 200 km s^{-1} and effective surface brightness I_e in 10^9 L$_\odot$ kpc^{-2}.

We follow the formalism presented by Kelly (2007) by modelling both $\log \sigma$ and $\log I_e$ as being drawn from multivariate Gaussian distributions with some mean μ and dispersion $\bar{\tau}$, and allowing
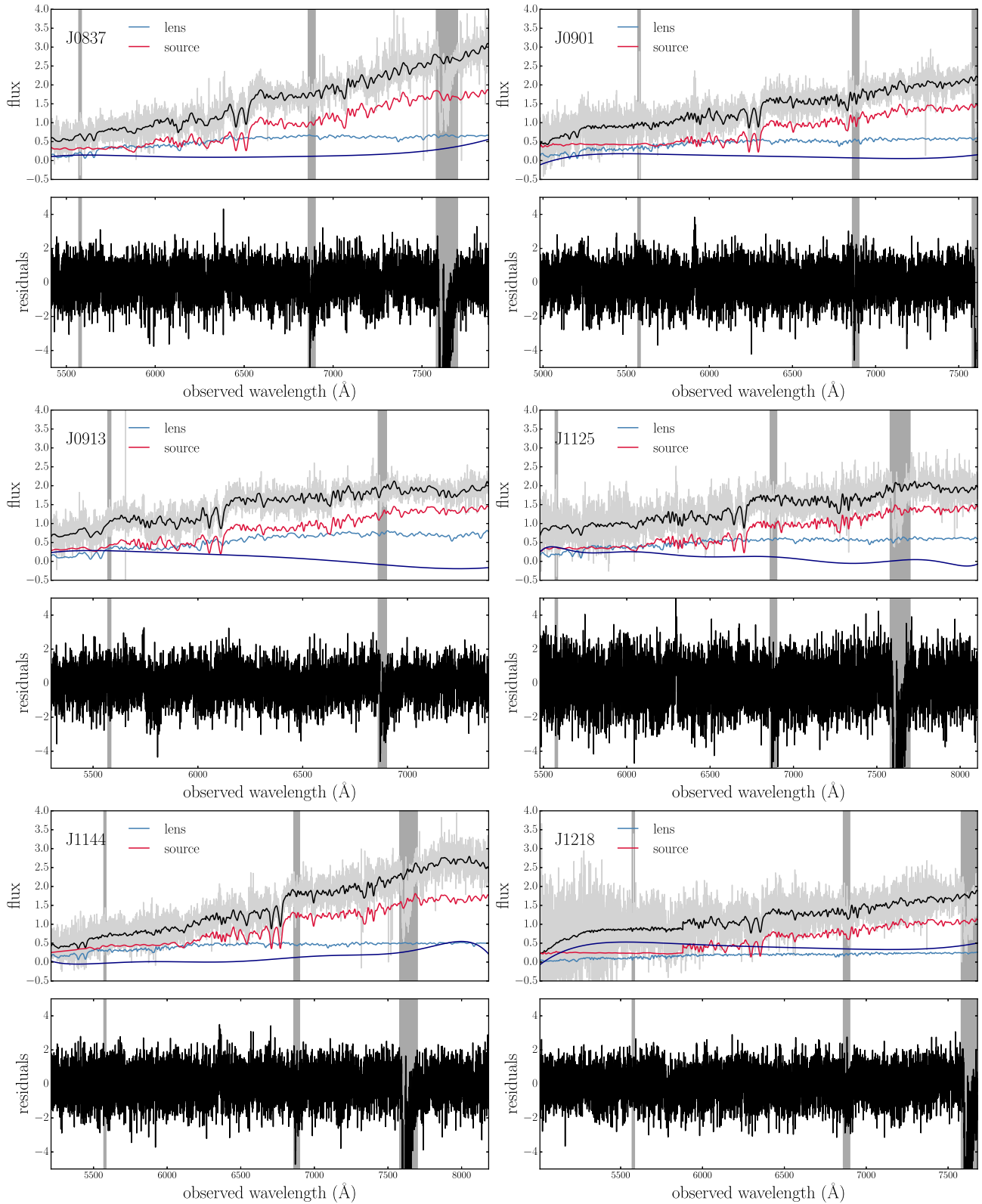
Figure 1. ESI/Keck spectra for the 12 EELs in our sample, with kinematic models overplotted. In the upper panels, the data are shown in grey, the total model spectrum in black and the contributions to the model from lens, source and continuum in blue, red and purple, respectively. The lower panels show the residuals of the kinematic models; vertical grey bands represent regions that were masked from the fit due to the presence of telluric absorption features.
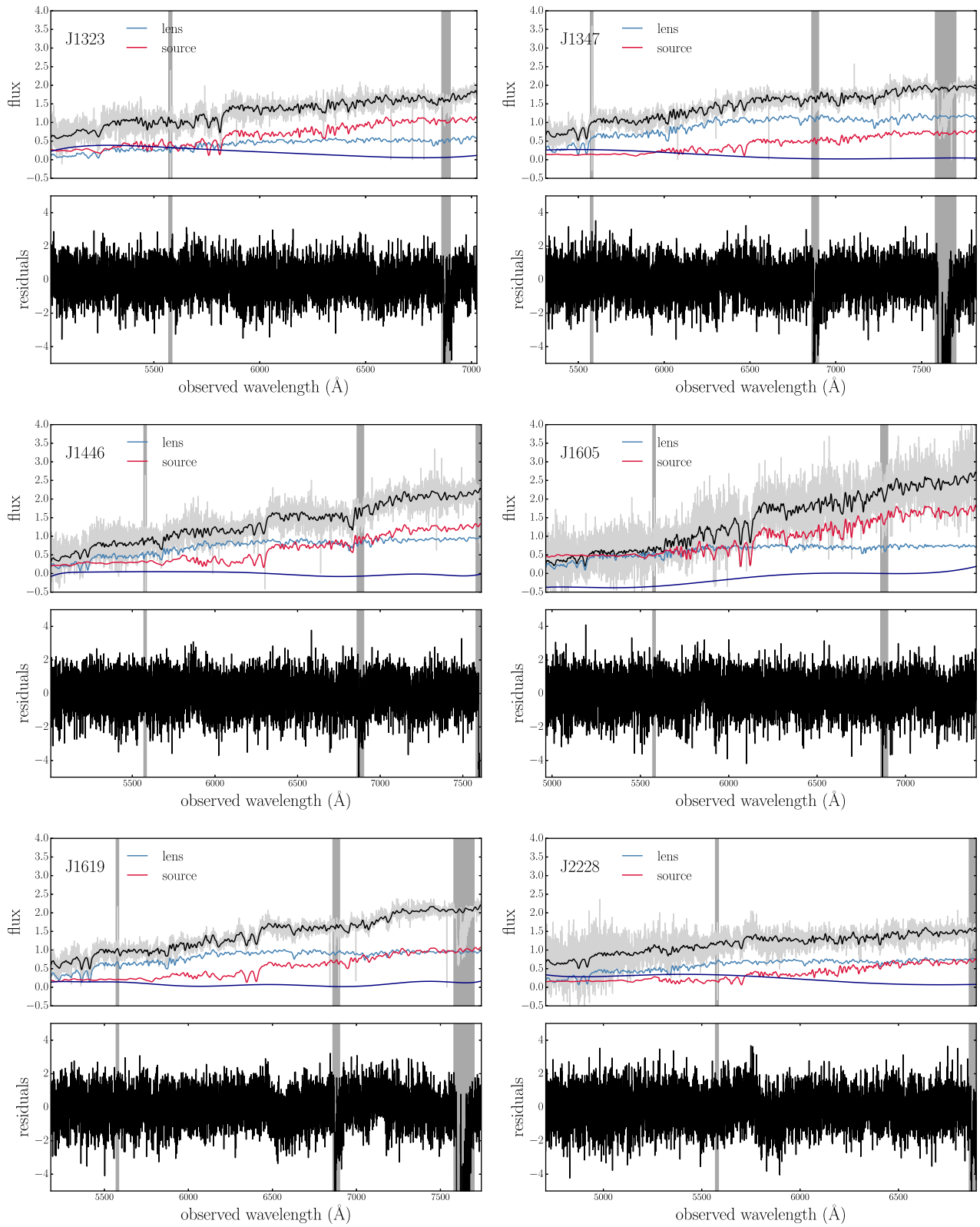
Figure 1 – *continued*

Table 1. FP data for the EELs source galaxies. Photometry is evaluated in the rest-frame Johnson *V* band using the photometric models presented in Oldham et al. (2017a), and kinematics are measured as described in Section 2.

EEL	R_e (kpc)	σ (km s^{-1})	$\log I_e$ (L$_\odot$ kpc^{-2})
J0837+0801	4.42 ± 0.27	253 ± 13	9.14 ± 0.01
J0901+2027	3.26 ± 0.19	205 ± 10	8.89 ± 0.01
J0913+4237	4.11 ± 0.17	193 ± 10	8.86 ± 0.01
J1125+3058	1.17 ± 0.02	182 ± 9	9.61 ± 0.01
J1144+1540	9.64 ± 0.28	225 ± 11	8.50 ± 0.02
J1218+5648	6.79 ± 0.33	191 ± 10	8.67 ± 0.01
J1323+3946	1.82 ± 0.11	162 ± 8	9.14 ± 0.01
J1347−0101	5.39 ± 0.49	152 ± 8	8.33 ± 0.02
J1446+3856	1.59 ± 0.04	207 ± 10	9.49 ± 0.01
J1605+3811	2.56 ± 0.05	160 ± 8	9.08 ± 0.01
J1619+2024	5.24 ± 0.20	283 ± 28	8.95 ± 0.01
J2228+2024	4.15 ± 0.08	149 ± 15	8.81 ± 0.01

some intrinsic scatter σ_{FP} along the direction of $\log R_e$; regarding the ongoing discussion on how to fit the FP (Hyde & Bernardi 2009), we note that this method is closer to the case of minimizing the residuals along $\log R_e$ rather than perpendicular to the plane. Full details on the form of the likelihood function can be found in Kelly (2007), but essentially, we construct the likelihood for the data

given a particular set of plane and parent distribution parameters, and obtain the posterior distribution using an MCMC exploration of the parameter space. The FP that we infer is shown in both side-on and face-on projections in Fig. 2 and our inference on the parameters is summarized in Table 2. As our sample is small, we test the robustness of our inference by remodelling random subsamples of the data set and find that the uncertainty introduced by this is small and less than half the size of the statistical uncertainties. We find that the observed FP of the EELs sources is steep relative to the FP of 'normal' galaxies, with $\alpha = 1.54 \pm 0.36$ as compared to the $\alpha = 1.24 \pm 0.07$ that is found locally, and $\beta = -0.68 \pm 0.06$ compared to the local value $\beta = -0.82 \pm 0.02$ (Jorgensen, Franx & Kjaergaard 1996); note though that both are consistent with the 'normal' FP parameters within 2σ. As a reference, we use the sample of 17 ETGs belonging to the $z = 0.545$ cluster MACSJ0717.5+3745 which were presented in Oldham et al. (2017b); these ETGs have a similar redshift and mean velocity dispersion to those in the EELs sample, but FP parameters that are consistent with the local values. Fig. 2 shows that these do indeed fall differently on the FP. We also note that Auger et al. (2010a) found that the inclusion of an intrinsic scatter around the FP further tilts the plane of normal ETGs along the $\log \sigma$ such that it is shallower than the Jorgensen et al. (1996) value (Auger et al. 2010a find $\alpha = 1.02 \pm 0.20$, 1.19 ± 0.14 with and without intrinsic scatter, respectively). We also find this to be the case, with the removal of an intrinsic scatter from
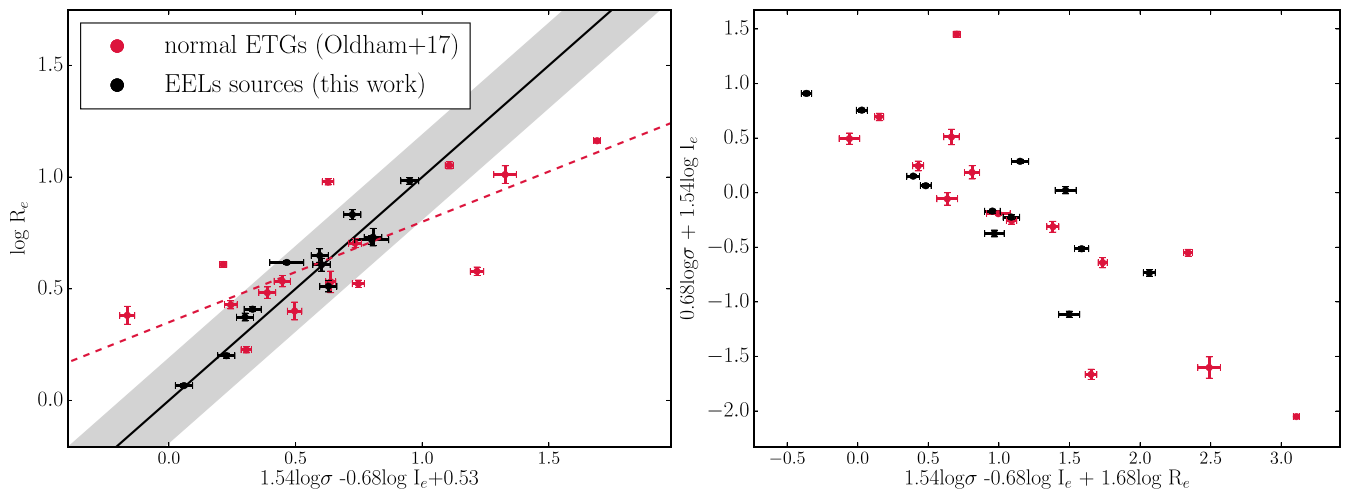
Figure 2. The observed FP of the massive compact EELs sources, shown in side-on (left) and face-on (right) projections, with the similar-redshift, less compact ETGs from Oldham, Houghton & Davies (2017b) shown in red for comparison. The FP is steeper in $\log \sigma$ and shallower in $\log I_e$ relative to that of the 'normal' Oldham et al. (2017b) galaxies, which indicates that both the dark and stellar mass structure and stellar populations vary as a function of the plane parameters. The FP also has a comparable intrinsic scatter to that of normal ETGs, implying that the intrinsic scatter is driven by stellar population properties. Velocity dispersions, surface brightnesses and effective radii are measured in units 200 km s^{-1}, 10^9 L$_\odot$ and kpc, respectively.

Table 2. Parameters and associated uncertainties for the Fundamental Plane, modelled according to the equation $\log R_e = \alpha \log \sigma + \beta \log I_e + \gamma$, with intrinsic scatter σ_{FP} about $\log R_e$. The independent variables $\log \sigma$ and $\log I_e$ are modelled as being drawn from Gaussian distributions with mean $\vec{\mu} = (\mu_\sigma, \mu_{I_e})$ and variance $\vec{\tau}^2 = [(\tau_\sigma^2, \rho\tau_\sigma\tau_{I_e}), (\rho\tau_\sigma\tau_{I_e}, \tau_{I_e})]$. Velocity dispersions, surface brightnesses and effective radii are measured in units 200 km s^{-1}, 10^9 L$_\odot$ and kpc, respectively. The first and second rows represent models with and without an intrinsic scatter; allowing for an intrinsic scatter makes the FP shallower in the $\log \sigma$ directions; the third and fourth rows represent the same, but after accounting for the bias introduced by the EELs source selection function. The selection has a negligible effect on the FP parameters.

	α	β	γ	μ_σ	μ_{I_e}	τ_σ	τ_{I_e}	ρ	$\log \sigma_{FP}$
Observed	1.54 ± 0.36	−0.68 ± 0.06	0.53 ± 0.02	0.00 ± 0.03	−0.03 ± 0.14	0.07 ± 0.02	0.38 ± 0.11	0.19 ± 0.32	−1.31 ± 0.19
	1.76 ± 0.29	−0.69 ± 0.04	0.56 ± 0.01	−0.02 ± 0.02	−0.04 ± 0.13	0.06 ± 0.02	0.39 ± 0.11	0.07 ± 0.31	−
Intrinsic	1.41 ± 0.35	−0.66 ± 0.06	0.56 ± 0.02	−0.02 ± 0.03	−0.02 ± 0.12	0.08 ± 0.02	0.35 ± 0.10	0.03 ± 0.30	−1.28 ± 0.18
	1.69 ± 0.28	−0.69 ± 0.04	0.56 ± 0.01	−0.01 ± 0.02	−0.03 ± 0.12	0.07 ± 0.02	0.37 ± 0.11	0.07 ± 0.30	−

our model giving $\alpha = 1.76 \pm 0.29$ (and having negligible effect on β).

The fact that these ETGs have compact light profiles means that their luminosity-weighted velocity dispersions probe only their very central regions, where the dark matter fraction is minimal. To the zeroth order, we might then expect that any deviation in their FP from the virial prediction must be due to variations in the stellar mass and dynamical structure across the plane, as opposed to variations in the dark matter. That we find their FP to be tilted relative to both the local ETG population *and* the virial plane indicates that the properties of both the stellar mass *and* the dark matter vary across the plane. However, before drawing conclusions from this, we must account for the effect of the selection function of the EELs sources on the FP parameters.

3.2 The intrinsic Fundamental Plane

The EELs sources form a biased population, as they were found in a lens search, and this may have a non-trivial effect on the orientation of the FP. We now follow the reasoning presented in Oldham et al. (2017a) to correct for this bias and so recover the *intrinsic* FP of these compact systems.

The selection function of the EELs sources has three main contributions. First, the source must be lensed by the foreground object; this relates to the cross-section for lensing. Secondly, the inclusion of an EEL in the SDSS spectroscopic sample requires the lens+source system as a whole to satisfy the criteria of the SDSS target selection (Strauss et al. 2002), which itself is non-trivial, though the main effect here is that the system is bright. Finally, the EEL must pass our spectroscopic search, which is subjective but imposes criteria such as the (magnified) source galaxy flux being comparable to the lens galaxy flux and the redshifts of the two objects approximately satisfying $0.1 \lesssim z \lesssim 0.7$. The combination of these conditions leads to some selection function that modifies the intrinsic population of compact galaxies to the population of EELs sources that we observe.

Of these three contributions, the latter two are difficult to quantify and should not introduce any large bias into our measurement of the FP, although they will push us to the high-surface-brightness end. On the other hand, the first – the lensing cross-section – introduces a selection function such that we are relatively more efficient at selecting compact galaxies at lower velocity dispersions. We can understand this as follows: differential magnification introduces a bias towards smaller objects (closer to the line of sight of the lens), whereas, for a given size, there is no bias as a function of luminosity, and therefore velocity dispersion (assuming the latter is dominated by stellar mass). The result of this is that an object of fixed velocity dispersion becomes increasingly likely to be seen in the lensed population relative to the intrinsic population as it becomes more compact.

This bias enters the FP in two ways, making its orientation biased towards objects with (a) small R_e and (b) large $\log I_e$. Following Oldham et al. (2017a), we modify our likelihood for the FP data for the *i*th EEL, given a model, by a function describing the magnification achieved by the lens as a function of source size $F_i(R_{e,i})$, which serves as a proxy for the probability of the source being identified in the lens search. The result is summarized in Table 2 for models with and without intrinsic scatter, and shows that the bias is negligible – probably because of the low intrinsic scatter, which makes selection effects unimportant – and the FP of these compact systems remains tilted relative to that of normal ETGs. As mentioned in Section 3.1, this seems to indicate that the structure of both the

dark and luminous mass components varies across the FP, i.e. as a function of mass. A discussion of this result is presented in Section 5.1.

4 PHYSICAL MODELS

We can also combine our kinematic measurements, which give a measure of the *total* mass in the central regions, with our photometric measurements from Oldham et al. (2017a), which give a measure of the *stellar* mass, to make inference on the central dark matter fraction. By further supplementing these measurements with abundance matching relations, we can develop toy models to reconstruct the dark halo on large scales and so investigate the dark structure. We emphasize that our data are only sensitive to the mass in the *central* regions, and that strong assumptions about how the stellar mass (which we can measure) relates to the virial mass (which we cannot measure) must be made. Nevertheless, abundance matching relations have been shown to be robust (Behroozi, Conroy & Wechsler 2010), and can therefore provide useful insight here, allowing us to probe the halo structure out to relatively high redshifts.

Our physical models are constructed as follows. For each EEL, we take the model of the lens system from Oldham et al. (2017a) and use the surface brightness profile $I(R)$ for the source to construct its stellar mass profile, assuming a stellar mass-to-light ratio which is set by the total magnitude and total stellar mass (under the assumption of either a Chabrier or a Salpeter IMF). We use a generalized Navarro–Frenk–White (gNFW) profile to construct the dark matter halo as

$$\rho(r) = \frac{\rho_0}{\left(\frac{r}{r_s}\right)^{\xi} \left(1 + \frac{r}{r_s}\right)^{3-\xi}}, \tag{2}$$

where the normalization $\rho_0(M_\star)$ is drawn from a normal distribution based on the $z = 0.6$ $M_{\rm halo}(M_\star)$ abundance matching relations of Behroozi, Wechsler & Conroy (2013); the inner density slope ξ is drawn from a normal distribution $\mathcal{N}(\mu_\xi, \tau_\xi^2)$ (such that μ_ξ characterises, the mean inner density slope of the EELs source population and τ_ξ represent their scatter) and the scale radius r_s is either calculated from the mass–concentration relation (Macciò, Dutton & van den Bosch 2008, though we note that this relation was constructed assuming NFW haloes, and it is not clear that it should still be valid when the NFW assumption is relaxed) or calculated from concentration distribution $\mathcal{N}(\mu_c, \tau_c^2)$ with μ_c, τ_c to be inferred. Though the NFW profile is commonly used due to its success in describing the dark haloes of galaxies in dark-matter-only simulations (Navarro, Frenk & White 1997), the use of the gNFW is motivated by the expectation that baryonic physics should modify the halo in some way – either contracting the halo via adiabatic processes, creating a super-NFW cusp $\xi > 1$ (Blumenthal et al. 1986; Gnedin et al. 2004), or hollowing it out via heating from active galactic nuclei or dynamical friction, leading to a sub-NFW central region $\xi < 1$ (e.g. El-Zant et al. 2004; Mashchenko, Couchman & Wadsley 2006; Governato et al. 2012; Laporte et al. 2012; Velliscig et al. 2014).

We then use the total density profile, $\rho(r) = \rho_{\rm DM}(r) + \rho_\star(r)$, to calculate a velocity dispersion using the spherical Jeans equation:

$$\frac{\mathrm{d}}{\mathrm{d}r} \left(l\sigma_r^2\right) + 2\frac{\beta(r)}{r}l\sigma_r^2 = l(r)\frac{GM(r)}{r^2}, \tag{3}$$

where $l(r)$ is the luminosity density of the stars (i.e. the deprojected surface brightness profile, assuming axisymmetry), $\beta(r) = 1 - \sigma_t^2/\sigma_r^2$ is the anisotropy parameter and $\sigma_r(r)$ the
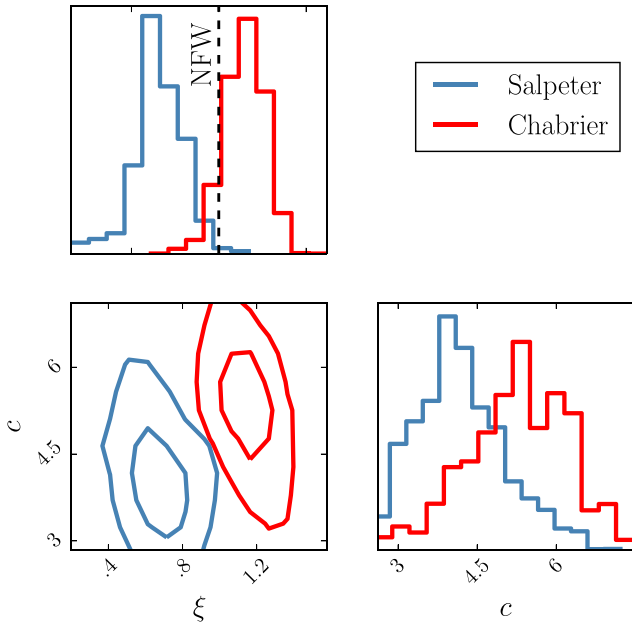
Figure 3. Inference on the structure of the dark halo for Chabrier (red) and Salpeter (blue) IMFs, compared to the expected inner slope from an NFW profile ($\xi = 1$; black dashed line). The measurement of the inner slope depends strongly on the form for the IMF that is assumed, with a bottom-heavy (Salpeter) IMF requiring less dark matter centrally than the NFW prediction and a bottom-light (Chabrier) IMF requiring more dark matter than the NFW prediction. An independent IMF probe is needed if we are to robustly distinguish between these scenarios; however, assuming that the EELs sources have Salpeter-like IMFs, consistent with previous IMF studies, implies the presence of sub-NFW haloes and points towards the action mergers and accretion in removing dark matter from the central regions.

radial velocity dispersion, which we then project along the line of sight as

$$\frac{1}{2} I(R)\sigma_{\mathrm{los}}(R)^2 = \int_R^\infty \frac{l\sigma_r^2 r\,\mathrm{d}r}{\sqrt{r^2 - R^2}} - R^2 \int_R^\infty \frac{\beta l \sigma_r^2\,\mathrm{d}r}{r\sqrt{r^2 - R^2}} \qquad (4)$$

to obtain the line-of-sight velocity dispersion $\sigma_{\mathrm{los}}(R)$ as a function of projected radius R. Finally, we integrate σ_{los} over a circular aperture of radius $1.5R_e$ (comparable to the effective aperture over which the lensed source spectra were extracted) to obtain the velocity dispersion that would be measured within the aperture

$$\sigma_{\mathrm{ap}}^2 = \frac{\int_0^{R_{\mathrm{ap}}} I\sigma_{\mathrm{los}}^2 R\,\mathrm{d}R}{\int_0^{R_{\mathrm{ap}}} I R\,\mathrm{d}R} \qquad (5)$$

(see e.g. Mamon & Łokas 2005). We investigate both isotropic and constant-anisotropy models across the range $-2 \le \beta \le 1$, and find that the difference is sufficiently small that our data cannot distinguish between them; we therefore adopt $\beta = 0$ in all models. Thus, given the luminous structure of an EELs source, we can reconstruct the halo and compare the implied central (dark+light) mass with the central velocity dispersion to constrain the dark matter structure in the inner regions.

Our inference is shown in Fig. 3 and Table 3. We find that our inference on the halo inner slope depends strongly on the IMF that is assumed, with bottom-heavy (Salpeter) and bottom-light (Chabrier) IMFs requiring haloes that are excavated and contracted, respectively. This is a common problem in attempts to disentangle the dark and luminous mass structure of ETGs and in general must

Table 3. Parameters and associated uncertainties for physical models of the dark matter mass structure, assuming a halo density profile as given in equation (2), with (a) free ξ and r_s determined from the mass–concentration relation, and (b) free ξ and concentration c, and assuming (a) Chabrier and (b) Salpeter IMFs. A Chabrier IMF requires the presence of more dark matter centrally than the NFW + abundance matching prediction; conversely, a Salpeter IMF requires less dark matter than the NFW + abundance matching prediction.

IMF	Free	μ_ξ	τ_ξ	μ_c	τ_c
Chabrier	ξ	$1.23^{+0.08}_{-0.09}$	$0.29^{+0.05}_{-0.08}$	–	–
	ξ, c	$1.15^{+0.11}_{-0.12}$	$0.32^{+0.11}_{-0.06}$	$5.34^{+0.86}_{-1.10}$	$0.51^{+0.45}_{-0.34}$
Salpeter	ξ	$0.71^{+0.13}_{-0.13}$	$0.45^{+0.12}_{-0.08}$	–	–
	ξ, c	$0.65^{+0.14}_{-0.11}$	$-0.46^{+0.09}_{-0.07}$	$4.10^{+0.89}_{-0.72}$	$0.40^{+0.38}_{-0.29}$

be broken through the use of multiple tracer populations or other mass probes (e.g. Newman et al. 2013; Oldham & Auger 2016). In this case, the construction of stellar population models from spectral absorption features would provide an independent probe of the IMF that would allow this degeneracy to be broken and will be the topic of a future work. However, we also note that high-mass ETGs have been shown to require Salpeter-like IMFs in general (e.g. Auger et al. 2010b; van Dokkum & Conroy 2010; Cappellari et al. 2012); though the EELs sources span a range in mass, we note that their masses are generally high, which here would imply the existence of sub-NFW haloes and the removal of dark matter from their central regions. We discuss this investigation further in Section 5.2.

5 DISCUSSION

5.1 The Fundamental Plane

The rotation of the nominal FP from the virial prediction follows from the fact that the virial plane assumes that

$$\frac{M_{\mathrm{tot}}}{L} = \mathrm{constant} \qquad (6)$$

across the ETG population, whereas, in reality,

$$\frac{M_{\mathrm{tot}}}{L} = \frac{M_{\mathrm{tot}}}{M_\star}\frac{M_\star}{L} \qquad (7)$$

with both terms on the right-hand side of equation (7) potentially dependent on other galaxy properties. In particular, the first term may vary across the plane if the dark or light mass structure is non-homologous, whilst the second term may vary due to non-homology in the stellar populations, such as the stellar age and IMF (though structural non-homology in the stellar mass may contribute to this term as well). The EELs sources are massive, compact ETGs, and their kinematics probe only with their central regions, where the dark matter contribution to the mass is minimal. In this study, we have exploited this fact to attempt to disentangle these two contributions to the FP tilt, and thus to the behaviour of M_{tot}/L across the population.

In Section 3, we found the FP of the EELs to be oriented *in between* the nominal FP and the virial plane (and marginally consistent with both, i.e. at the 2σ level). Due to the low dark matter fractions in the centres of these systems (the kinematics imply masses within the effective radius on average 40 per cent larger than the Chabrier stellar masses but 17 per cent *smaller* than the Salpeter stellar masses, and previous studies indicate that Salpeter-like IMFs might be expected in these massive ETGs), this has implications for our understanding of ETGs as a population. First, the rotation of the
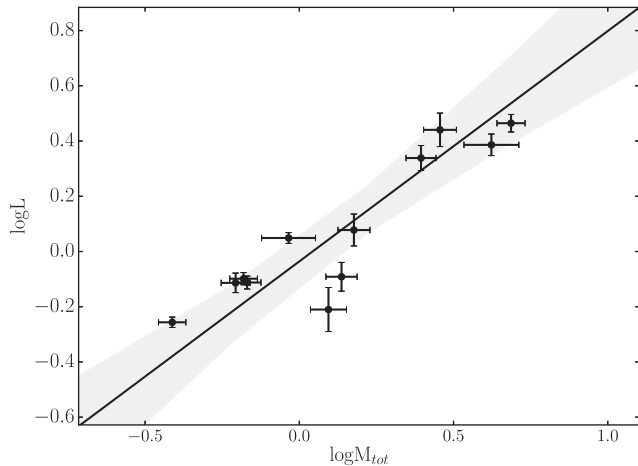
Figure 4. The mass–luminosity relation for the EELs sources, with $\log M_{\rm tot} = 2 \log \sigma + \log R_{\rm e} - 5$ and $\log L = \log I_{\rm e} + 2 \log R_{\rm e} - 10$ for σ in km s^{-1}, $I_{\rm e}$ in L$_\odot$ kpc^{-2} and $R_{\rm e}$ in kpc (note that, in each case, a constant is subtracted from each axis to minimize covariance between the inferred intercept and slope). As with the FP, this relation for the EELs sources lies in between expectations based on the virial plane and the nominal FP and suggests that the low dark matter fractions of the EELs sources removes some, but not all, of the systematic trends in $M_{\rm tot}/L$ that occur across the ETG population.

FP cannot be explained entirely by a mass-dependent dark matter fraction. If the rotation of the FP was solely due to mass-dependent dark matter fractions, then the low dark matter fractions of the EELs sources should cause their FP to be nearly aligned with the virial plane; that this is not the case implies that baryonic properties must also be mass dependent. Conversely, if the FP tilt were solely due to mass-dependent baryonic properties, then the EELs FP should be aligned with the nominal FP. The fact that this is not the case either indicates, then, that *ETGs are non-homologous in both their dark and their luminous properties.* Previously, Bolton et al. (2008) showed that the FP tilt for the sample of ETGs spanning a similar mass range could be explained entirely by deviations from *structural* homology, as opposed to deviations from *dynamical* homology, though they were unable to disentangle the relative importance of the contributions from the dark and luminous mass components. Interpreting our result in the light of that study, we can update our conclusion above to say that ETGs are non-homologous in both their dark and their luminous *mass structures.*

We underline this result by further constructing the relation between mass, $\log M \propto 2 \log \sigma + \log R_{\rm e}$, and luminosity, $\log L \propto \log I_{\rm e} + 2 \log R_{\rm e}$, in Fig. 4. This projection of the FP is edge-on for both the virial plane and the nominal FP, such that $\log L \propto \log M$ corresponds to the virial plane (as follows from equation 6) and $\log L \propto 0.75 \log M$ is consistent with the local FP parameters (Jorgensen et al. 1996). We fit a linear relation between $\log M$ and $\log L$ following the methods of Section 3, and find a slope $\alpha_{\rm LM} = 0.85 \pm 0.21$, which is also shown in Fig. 4. As with the FP, this result places the $\log L$–$\log M$ relation in between the virial plane and the nominal FP expectations, and seems to confirm the idea that the low dark matter fractions of the EELs sources removes some, but not all, of the systematic trends in $M_{\rm tot}/L$ that occur across the ETG population. We note, however, that larger samples of lensed (or low redshift) compact ETGs are needed in order to make stronger claims in this regard.

We also note the difference in the FP of these compact ETGs from that of cluster ETGs at similar redshifts. In Oldham et al. (2017b),

we presented the FP of massive ETGs in the cluster MACSJ0717 at $z = 0.545$; this sample has the same mean velocity dispersion as the EELs sources ($\mu_\sigma \sim 200$ km s^{-1}), but their FP is extremely consistent with that of local ETGs, with no evidence for a tilt (see Fig. 2). The main implication of this result is that these cluster ETGs have already experienced the majority of their structural evolution by $z \sim 0.5$; contrary to the EELs sources, which have remained compact. In Oldham et al. (2017a), we also showed that the EELs sources do not appear to occupy unusually dense environments. Taken together, this pair of results is interesting as it provides further evidence for the accelerated growth of galaxies in dense environments: if any massive compact galaxies existed in MACSJ0717, they would be some of the brightest ETGs in the cluster and so should have been included in that study. The fact that they are not suggests that all the initially compact ETGs in that dense environment have already evolved into larger systems like those we see locally, whereas the EELs sources, in less dense environments, remain at an earlier stage of their evolution. To make a more quantitative statement here would require a thorough characterization of the selection functions of these two samples; nevertheless, this direct comparison strongly highlights the differences between these two populations.

Finally, we measure the FP to have a small scatter, $\log \sigma = -1.31 \pm 0.19$, comparable to that of the normal FP (Auger et al. 2010a find the SLACS lenses to have $\sigma = 0.049 \pm 0.009$). If scatter in the dark and the light structure contributed equally to the overall FP scatter, then we would expect to find a reduced intrinsic scatter in the FP of the EELs sources, where the low dark matter fractions should make the contribution to the scatter from the dark matter minimal. The fact that the intrinsic scatter is not decreased when variations in the dark matter are effectively removed in this way implies that this scatter is largely due to variations in the stellar structure and stellar populations, and that the dark matter structure in ETGs – at least in their central regions – is subject to less variation. Equally, though, our sample size is small, which makes statistical properties of the sample, such as the intrinsic scatter, subject to uncertainty.

5.2 Physical models

In Section 4, we constructed toy models for the mass structure in the EELs sources in order to probe their dark matter distributions. Since we cannot currently constrain the IMFs in these systems, we constructed these models assuming a universal IMF which is either Chabrier and Salpeter and found that the inference on the halo structure is (perhaps unsurprisingly) very sensitive to the choice of IMF. If a Chabrier-like IMF is assumed, we find the sources to require *more* dark matter in the centre than implied by the abundance matching+NFW prediction, whereas the use of a more bottom-heavy Salpeter IMF requires *less* dark matter centrally than the abundance matching+NFW prediction. These two results are very different and imply correspondingly different physics: whilst a sub-NFW dark halo would imply the action of either strong AGN feedback or merger processes in removing dark matter from the centre, a super-NFW halo would indicate an important role for initial adiabatic processes during galaxy assembly. It might be possible to distinguish between these scenarios by using higher signal-to-noise spectra to independently constrain the IMF in these systems via stellar population modelling, though the difficulty here would be in robustly measuring the continuum, given that the spectra contain the light from both the lens and the source galaxies. This is something we will explore in a future work.

For now, however, we combine a number of recent developments in our understanding of ETGs to sketch a feasible picture of the structure and evolution of the galaxies in our sample. At the outset, we emphasize our assumption that all the galaxies in our sample have the same IMF: in reality, their mass range may imply a variation in the IMF across the sample, which would complicate the following picture; nevertheless, given that the non-universality of the IMF remains not well understood and that we cannot constrain the IMF from our data, we adopt this as a reasonable first model.

First, existing evidence suggests that ETGs of comparable stellar mass to the EELs sources require bottom-heavy IMFs (e.g. Auger et al. 2010b; van Dokkum & Conroy 2010; Cappellari et al. 2012), and further, that the IMF of ETGs may be most bottom-heavy in their central regions (Martín-Navarro et al. 2015; Oldham et al. 2017c). Seen in the context of the inside-out growth scenario, in which ETGs grow in two stages by the formation of a compact core at high redshifts, followed by the accretion of lower mass systems at large radii to form an extended envelope, this suggests that the formation of the initial core may occur in fundamentally different star formation conditions from the lower mass systems that it subsequently accretes. In this picture, the EELs sources, which seem to have experienced very little accretion so far, should have very bottom-heavy IMFs, comparable with the most central regions of local ETGs. As shown in Fig. 3, this would then imply that their halo profiles are sub-NFW. What is interesting about this is that one of the most promising mechanisms for the removal of dark matter from the inner regions of ETG haloes is dynamical friction from infalling satellites during merger events, which has been shown in simulations to be effective at transferring energy from the infalling objects to the halo and therefore causing the latter to expand (Laporte et al. 2012).

In Oldham et al. (2017a), we revealed evidence for ongoing merger activity in the *luminous* structure of these systems in the form of faint envelopes surrounding their compact cores; the possibility that they also have sub-NFW haloes may therefore present further evidence for their growth by mergers and accretion. This independent evidence, based on their *dark* structure, provides further insight into their evolution and presents new potential evidence for the importance of dry merging in the growth of ETGs.

6 CONCLUSIONS

We have presented and modelled spectra and the resulting stellar kinematics for 13 EELs to explore the nature of the FP and the dark and light mass structure of the source galaxies. Our main conclusions are as follows.

(i) Relative to normal ETGs, the FP of the EELs sources is tilted towards, but still inconsistent with, the virial plane. Since the EELs sources are compact systems with small effective radii, their luminosity-weighted kinematics probe the very central regions where the dark matter fraction is low; this means their FP is sensitive predominantly to their *luminous* material, as opposed to their *dark matter*. The fact that their FP is rotated relative to both the FP of normal galaxies and the virial plane indicates that the properties of both the stellar populations and the dark matter are responsible for the well-known FP tilt, i.e. vary as a function of galaxy mass.

(ii) The intrinsic scatter of the FP of the EELs sources is small ($\log \sigma = -1.31 \pm 0.19$), but comparable to that of the FP of normal galaxies. This implies that variations in the inner dark matter structure do not contribute significantly to the scatter, which must instead be driven by scatter in the stellar properties.

(iii) The halo structure can only be constrained, in the context of well-motivated models, when a universal IMF is assumed. However, on the basis of mounting evidence that massive, compact ETGs should have bottom-heavy IMFs, these galaxies appear to be best characterized by a dark matter halo with a sub-NFW inner density slope. This is consistent with a picture in which these galaxies are growing by successive mergers and accretion of smaller objects, and may therefore provide further evidence for their inside-out growth.

REFERENCES

Auger M. W., Treu T., Bolton A. S., Gavazzi R. Koopmans L. V. E., Marshall P. J., Moustakas L. A., Burles S., 2010a, ApJ, 724, 511
Auger M. W., Treu T., Gavazzi R., Bolton A. S. Koopmans L. V. E., Marshall P. J., 2010b, ApJ, 721, L163
Behroozi P. S., Conroy C., Wechsler R. H., 2010, ApJ, 717, 379
Behroozi P. S., Wechsler R. H., Conroy C., 2013, ApJ, 770, 57
Blumenthal G. R., Faber S. M., Flores R., Primack J. R., 1986, ApJ, 301, 27
Bolton A. S., Treu T., Koopmans L. V. E., Gavazzi R. Moustakas L. A., Burles S., Schlegel D. J., Wayth R., 2008, ApJ, 684, 248
Bruzual G., Charlot S., 2003, MNRAS, 344, 1000
Cappellari M. et al., 2006, MNRAS, 366, 1126
Cappellari M. et al., 2012, Nature, 484, 485
Ciotti L., Lanzoni B., Renzini A., 1996, MNRAS, 282, 1
Daddi E. et al., 2005, ApJ, 626, 680
Djorgovski S., Davis M., 1987, ApJ, 313, 59
Dressler A., Lynden-Bell D., Burstein D., Davies R. L., Faber S. M., Terlevich R., Wegner G., 1987, ApJ, 313, 42
El-Zant A. A., Hoffman Y., Primack J., Combes F., Shlosman I., 2004, ApJ, 607, L75
Foreman-Mackey D., Hogg D. W., Lang D., Goodman J., 2013, PASP, 125, 306
Gnedin O. Y., Kravtsov A. V., Klypin A. A., Nagai D., 2004, ApJ, 616, 16
Governato F. et al., 2012, MNRAS, 422, 1231
Hyde J. B., Bernardi M., 2009, MNRAS, 396, 1171
Jorgensen I., Franx M., Kjaergaard P., 1996, MNRAS, 280, 167
Kelly B. C., 2007, ApJ, 665, 1489
La Barbera F., Busarello G., Merluzzi P., de la Rosa I. G. Coppola G., Haines C. P., 2008, ApJ, 689, 913
Laporte C. F. P., White S. D. M., Naab T., Ruszkowski M., Springel V., 2012, MNRAS, 424, 747
Macciò A. V., Dutton A. A., van den Bosch F. C., 2008, MNRAS, 391, 1940

Mamon G. A., Łokas E. L., 2005, MNRAS, 363, 705
Martín-Navarro I., Barbera F. L., Vazdekis A., Falcón-Barroso J., Ferreras I., 2015, MNRAS, 447, 1033
Martizzi D., Teyssier R., Moore B., 2013, MNRAS, 432, 1947
Mashchenko S., Couchman H. M. P., Wadsley J., 2006, Nature, 442, 539
Navarro J. F., Frenk C. S., White S. D. M., 1997, ApJ, 490, 493
Newman A. B., Treu T., Ellis R. S., Sand D. J., 2013, ApJ, 765, 25
Newman A. B., Ellis R. S., Treu T., 2015, ApJ, 814, 26
Oldham L. J., Auger M. W., 2016, MNRAS, 457, 421
Oldham L. et al., 2017a, MNRAS, 465, 3185
Oldham L. J., Houghton R. C. W., Davies R. L., 2017b, MNRAS, 465, 2101
Oldham L. et al., 2017c, MNRAS, in press
Read J. I., Gilmore G., 2005, MNRAS, 356, 107
Sheinis A. I., Bolte M., Epps H. W., Kibrick R. I. Miller J. S., Radovan M. V., Bigelow B. C., Sutin B. M., 2002, PASP, 114, 851

Strauss M. A. et al., 2002, AJ, 124, 1810
Trujillo I., Burkert A., Bell E. F., 2004, ApJ, 600, L39
Trujillo I. et al., 2006, MNRAS, 373, L36
van Dokkum P. G., Conroy C., 2010, Nature, 468, 940
van Dokkum P. G. et al., 2008, ApJ, 677, L5
Valdes F., Gupta R., Rose J. A., Singh H. P., Bell D. J., 2004, ApJS, 152, 251
Velliscig M., van Daalen M. P., Schaye J., McCarthy I. G., Cacciato M., Le Brun A. M. C., Vecchia C. D., 2014, MNRAS, 442, 2641

This paper has been typeset from a TEX/LATEX file prepared by the author.